

A Study of the Numerical Instability of the AUSM Scheme

Sutthisak Phongthanapanich*

Department of Mechanical Engineering Technology, College of Industrial Technology,
King Mongkut's University of Technology North Bangkok, Bangkok 10800, Thailand

Abstract

This paper presents a study of the numerical instability of the Advection Upstream Splitting Method (AUSM) for inviscid compressible flow analysis on two-dimensional structured triangular grids. The composition of the AUSM flux-vector splitting scheme for the solution of the Euler equations is reviewed. Mach number splitting functions operating with values from adjacent cells are used to determine numerical convective fluxes, and the pressure splitting is used for the evaluation of numerical pressure fluxes. The scheme is further extended to obtain higher-order spatial and temporal solution accuracy. A computational model for shock wave problems is presented to investigate the numerical stability of the scheme. The performance and efficiency of the AUSM scheme are evaluated by solving three high-speed compressible flow problems.

Keywords: AUSM Scheme; Explicit Scheme; Higher-order Scheme; Numerical Instability.

1. Introduction

In general, fluids are naturally compressible. A fluid whose density varies an appreciable amount under high pressure load is called a compressible fluid. The main difference between compressible and incompressible fluids is the rate at which forces are transmitted through the fluid itself [1]. Compressible flow behavior that includes shock waves occurs in numerous situations. The problem of a fixed shock in a steady flow can simply be modeled, and its solution obeys the Rankine-Hugoniot relationships. A pressure disturbance is transmitted in the form of successive compression and rarefaction waves due to its elastic in nature. When the strength of a pressure disturbance becomes large enough, the speed of the wave may increases beyond the speed of a sound wave, and this generates a wave of a higher

amplitude called a shock wave. A shock tube is an equipment for generating gas flows of a very short duration which commonly used to generate shock or blast waves in the laboratory. A rapid removal of the diaphragm generates a flow of a short duration containing waves of finite amplitude separated by quasi-steady regions. Initially, a shock wave travels into the low pressure gas while an expansion or rarefaction wave travels into the high pressure gas. The quasi-steady flow regions induced behind these waves are separated by a contact surface across which pressure and velocity are equal.

During the past decades, a variety of shock-capturing schemes have been developed for solving the Euler equations of gas dynamics. The growth of interest in computational fluid dynamics especially the upwind schemes brought the development of

* Correspondence: sutthisakp@kmutnb.ac.th

sufficiently robust, accurate and efficient numerical methods for the solution of inviscid compressible flow problems described by the non-linear system of the Euler equations. One of the methods, the Roe's flux-difference splitting scheme [2] has been proven to provide good efficiency for the solution of compressible inviscid flow problems. However, the scheme has some weakness and may fail or produce unphysical numerical solutions for certain problems, such as the high Mach number flow past a blunt-body [3] and the moving shock in a straight duct from an odd-even grid perturbation [4]. The unrealistic phenomenon is known as the carbuncle phenomenon. Such phenomenon was first reported by Perry and Imlay [3] for a blunt-body computations using the Roe's FDS scheme. It consists of a spurious steady-state solution obtained when computing supersonic flows past a blunt-body problem. The spurious solution includes a recirculation region behind the detached bow shock in the vicinity of the stagnation line. To overcome this problem, many researchers [5-9] proposed the entropy fix formulation to correct the near zero eigenvalues by some tolerances. However, There is an evidence [10] showing that the carbuncle phenomenon is incurable because it can be a valid solution with vanishing viscosity limits.

The upwind schemes are categorized as either flux-vector splitting (FVS) or flux-difference splitting (FDS). The FVS schemes [11-12] are known to be fast, simple and robust for capturing strong shocks and rarefaction waves. However, many numerical simulations indicated that these schemes are too dissipative and may deteriorate the boundary layer profiles. The FDS scheme by Roe [2] is widely used due to its accuracy, quality and mathematical clarity, while the FDS scheme requires longer computational time as compared to the FVS scheme due to its matrix calculations basis. The AUSM scheme was presented [13] as a simple, fast

and robust method in comparison to existing numerical schemes and became one of the most popular computational fluid dynamics techniques. The AUSM scheme is developed by combining the accuracy of the flux difference splitting scheme (FDS) and the robustness of flux vector splitting scheme (FVS) together. Accuracy was improved especially on the boundary or in the shear layers.

The objective of this work is to review the finite volume formulation of the first- and second-order accurate of the AUSM scheme on two-dimensional triangular grids. The numerical instability of the AUSM scheme on two-dimensional structured triangular grids is investigated by testing against some well-known problems that exhibit numerical shock instabilities. In order to improve the accuracy, Mach number and pressure splitting functions are used in this AUSM scheme (AUSM-M). The performance of the scheme is then evaluated through three examples. These examples are (1) the symmetric rarefaction wave, (2) the Mach 3 flow over forward facing step, and (3) the Mach 2 shock reflection over wedge problems.

2. Governing Equation and AUSM Scheme

The governing differential equations of the Euler equations for the two-dimensional inviscid flow [2] are given by

$$\frac{\partial \mathbf{U}}{\partial t} + \frac{\partial \mathbf{E}}{\partial x} + \frac{\partial \mathbf{G}}{\partial y} = 0 \quad (1)$$

where \mathbf{U} is the vector of conservation variables, \mathbf{E} and \mathbf{G} are the vectors of the convection fluxes in x and y directions, respectively. The perfect gas equation of state is in the form,

$$p = \rho e(\gamma - 1) \quad (2)$$

where p is the pressure, ρ is the density, e is the internal energy, and γ is the specific heat ratio (1.4 for perfect gas). By integrating Eq. (1) over a control volume, Ω , and by applying the divergence theorem to the resulting flux integral, we obtain

$$\frac{\partial}{\partial t} \int_{\Omega} U d\Omega + \int_{\partial\Omega} \mathbf{F} \cdot \hat{\mathbf{n}} dS = 0 \quad (3)$$

where $\mathbf{F} = E\hat{\mathbf{n}}_x + G\hat{\mathbf{n}}_y$ is the numerical flux vector and $\hat{\mathbf{n}}$ is the normal unit vector to the cell boundary. The underlying idea of the scheme is based on the recognition that the vector of convective fluxes [13] consists of two physically distinct parts, namely the convective and the pressure terms, that is

$$\mathbf{F} = V \begin{bmatrix} \rho \\ \rho u \\ \rho v \\ \rho H \end{bmatrix} + p \begin{bmatrix} 0 \\ n_x \\ n_y \\ 0 \end{bmatrix} \quad (4)$$

where H is the enthalpy, and V is the contravariant velocity for convecting the convective term as passive scalar quantities. On the other hand, the pressure flux term is governed by the acoustic wave speed.

By discretizing these two fluxes separately [13] and by introducing the advection Mach number for robustness, the numerical fluxes through a cell face can be written as

$$\mathbf{F}_{1/2}^C = M_{1/2} \begin{bmatrix} \rho a \\ \rho a u \\ \rho a v \\ \rho a H \end{bmatrix}_{L/R} \quad (5)$$

$$\mathbf{F}_{1/2}^p = p_{1/2} \begin{bmatrix} 0 \\ n_x \\ n_y \\ 0 \end{bmatrix} \quad (6)$$

where a is the speed of sound, and

$$(\bullet)_{1/2} = \begin{cases} (\bullet)_L & \text{if } M_{1/2} \geq 0 \\ (\bullet)_R & \text{if } M_{1/2} < 0 \end{cases} \quad (7)$$

Similar to the Van Leer's flux-vector splitting scheme [12], the advection Mach number is determined as a contribution of the left and right split Mach numbers by

$$M_{1/2} = M_L^+ + M_R^- \quad (8)$$

where the split Mach numbers are defined as

$$M^\pm = \begin{cases} \pm \frac{1}{4}(M \pm 1)^2 & \text{if } |M| \leq 1 \\ \frac{1}{2}(M \pm |M|) & \text{otherwise} \end{cases} \quad (9)$$

and the pressure at a cell face of the control volume is obtained from the second order splitting idea depending on the Mach number) as

$$p_{1/2} = p_L^+ + p_R^- \quad (10)$$

$$p^\pm = \begin{cases} \frac{p}{4}(M \pm 1)^2(2 \mp M) & \text{if } |M| \leq 1 \\ \frac{p}{2}(M \pm |M|)/M & \text{otherwise} \end{cases} \quad (11)$$

The distributions of the M^\pm and the p^\pm terms are shown in Figs. 1(a)-(b).

Finally, the numerical fluxes at the cell face of the AUSM scheme can be written in the upwind form as,

$$\mathbf{F}_{1/2} = \frac{1}{2} \mathbf{M}_{1/2} \left\{ \begin{bmatrix} \rho a \\ \rho a u \\ \rho a v \\ \rho a H \end{bmatrix}_L + \begin{bmatrix} \rho a \\ \rho a u \\ \rho a v \\ \rho a H \end{bmatrix}_R \right\} - \frac{1}{2} |\mathbf{M}_{1/2}| \left\{ \begin{bmatrix} \rho a \\ \rho a u \\ \rho a v \\ \rho a H \end{bmatrix}_R - \begin{bmatrix} \rho a \\ \rho a u \\ \rho a v \\ \rho a H \end{bmatrix}_L \right\} + \mathbf{P}_{1/2} \begin{bmatrix} 0 \\ n_x \\ n_y \\ 0 \end{bmatrix} \quad (12)$$

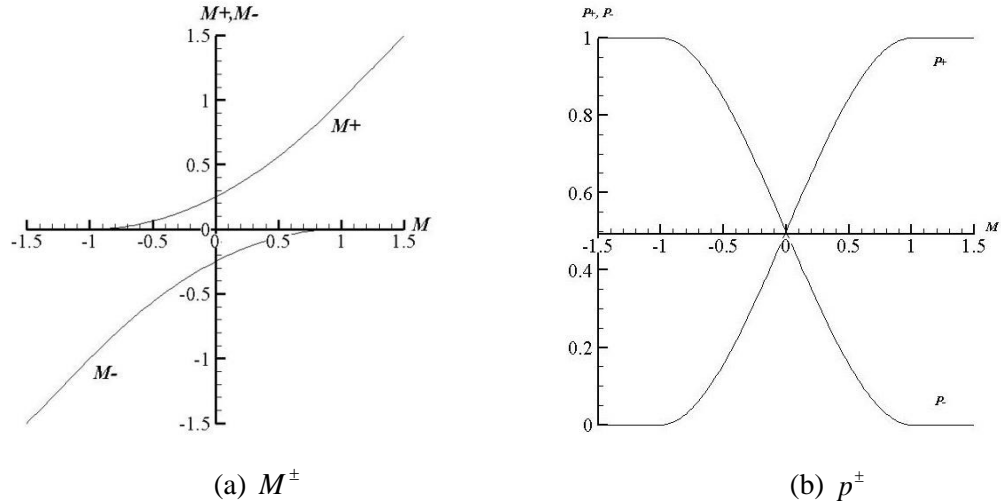


Fig. 1. Distribution of M^\pm and p^\pm terms.

By writing the numerical fluxes in this form, it is easy to emphasize that the convective term is convective by the normal Mach number ($M_{1/2}$) as passive scalar quantities, and the pressure flux term is governed by the acoustic wave speed ($p_{1/2}$).

3. Higher-order Extension

The solution accuracy from the first-order formulation described in the preceding section can be improved by implementing a high-order formulation for both space and time. A high-order spatial discretization is achieved by applying the Taylor' series expansion to the cell-centered solution for each cell face [14] which can be reconstructed from,

$$\mathbf{q}_{face} = \mathbf{q}_{centroid} + \psi \nabla \mathbf{q} \cdot \mathbf{r} \quad (13)$$

where $\mathbf{q} = [\rho \ u \ v \ p]^T$ consists of the primitive variables of the density, the velocity components, and the pressure, respectively; $\nabla \mathbf{q}$ represents the gradient of the variables; and \mathbf{r} is the vector projected to the given cell face. The quantity ψ in Eq. (13) represents the limiter for preventing spurious oscillation that may occur in the region of high gradients. In this study, the Vekatakrishnan's limiter function [15] is selected and can be written in the form,

$$\Psi_c = \min_{i=1,2,3} \begin{cases} \phi \left(\frac{\Delta_{+,max}}{\Delta_-} \right) & , \Delta_- \geq 0 \\ \phi \left(\frac{\Delta_{+,min}}{\Delta_-} \right) & , \Delta_- < 0 \\ 1 & , \Delta_- = 0 \end{cases} \quad (14)$$

where $\Delta_- = \mathbf{q}_c - \mathbf{q}_i$, $\Delta_{+,max} = \mathbf{q}_{max} - \mathbf{q}_i$, and $\Delta_{+,min} = \mathbf{q}_{min} - \mathbf{q}_i$. The \mathbf{q}_{max} and \mathbf{q}_{min} are respectively the maximum and minimum values of all distance-one neighboring cells. The function ϕ is expressed in the form

$$\phi(y) = \frac{y^2 + 2y}{y^2 + y + 2}. \quad (15)$$

Finally, the second-order temporal accuracy is achieved by implementing the second-order accurate Runge-Kutta time stepping method [16] as,

$$\begin{aligned} \mathbf{U}_i^* &= \mathbf{U}_i^n - \frac{\Delta t}{\Omega_i} \sum_{j=1}^3 \mathbf{F}^n \cdot \mathbf{n}_j \\ \mathbf{U}_i^{n+1} &= \frac{1}{2} \left[\mathbf{U}_i^0 + \mathbf{U}_i^* - \frac{\Delta t}{\Omega_i} \sum_{j=1}^3 \mathbf{F}^* \cdot \mathbf{n}_j \right] \end{aligned} \quad (16)$$

where Δt is the time step.

4. Numerical Examples

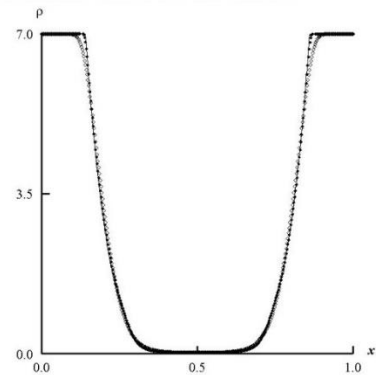
In order to evaluate the robustness and the accuracy of the AUSM scheme, three examples are examined. All examples presented in this section are tested using uniform triangular grids. These examples are (1) the symmetric rarefaction wave, (2) the Mach 3 flow over forward facing step, and (3) the Mach 2 shock reflection over wedge problems.

4.1 Symmetric Rarefaction Wave

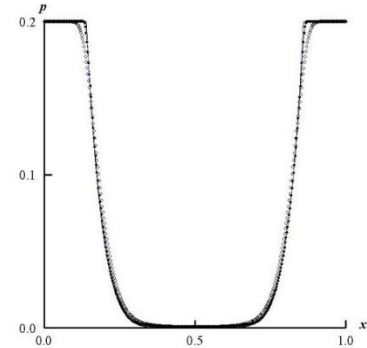
The first benchmark problem is a rather difficult case because the initial conditions are chosen to produce a vacuum at the central region of the domain. Many numerical schemes cannot preserve the contact discontinuity and require certain numerical fluxes corrections [9]. This problem [17] is simulated on a 1×0.1 domain, which is discretized by uniform triangular elements (400×40). The initial conditions of the

symmetric rarefaction wave problem ($M = 5$) are given by $(\rho, u, p)_L = (7, -1, 0.2)$ and $(\rho, u, p)_R = (7, 1, 0.2)$, such that they produce a vacuum at the center of domain.

Figures 2(a)-(c) show the first- and second-order accurate density, the pressure and the u -velocity distributions along the tube length at time $t = 0.3$ compared to the exact solutions. The first-order accurate solutions are shown by the hollow circle symbol. They are too diffusive and provide little accuracy especially in the vicinity of the rapid change area. This problem was repeated using the higher-order accurate scheme, and the solutions are shown by the solid circle symbol in Figs. 2(a)-(c). The distributions show that such higher-order extension of AUSM scheme can provide a more accurate solution than the first-order solution.



(a) Density



(b) Pressure

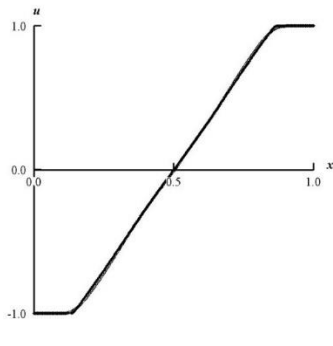


Fig.2. Comparison of exact and numerical solutions of problem 4.1.

4.2 Mach 3 Flow over Forward Facing Step

The second problem is a Mach 3 flow through the channel with a forward facing step. The flow exits through the right boundary as shown in Fig. 3. This problem was studied extensively by Woodward and Colella [18] and later by many researchers. Because the facing step contains a singularity, this may lead to an erroneous entropy layer at the downstream bottom wall as well as a spurious Mach stem at the bottom wall [19]. The flow phenomenon starts from the first time step. A strong shock wave is generated due to the facing step. Then, the shock wave impinges on the top wall and reflects at the wall to exhibit shock wave reflections at the top and bottom walls.

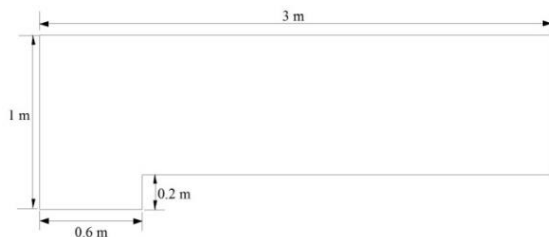


Fig.3. Problem geometry of problem 4.2.

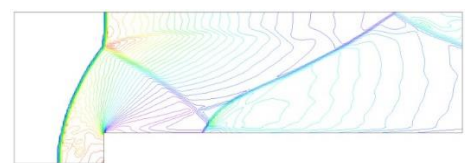
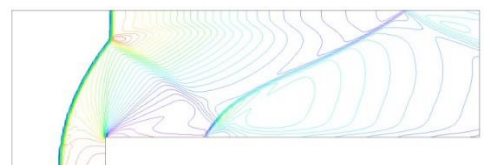


Fig.4. Density contours of problem 4.2.

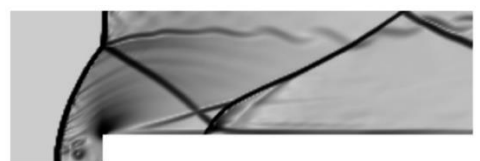


Fig.5. Schlieren plot of problem 4.2.

In the computation, the uniform triangular grid size of $1/20$ is used. Figures 4(a)-(b) show the first- and second-order accurate density contours at time $t = 10.5$ s. These figures show that the first-order accurate solution is diffusive compared to the second-order accurate solution. Again, the AUSM scheme can provide the improved resolution especially at the upper slip line emanated from the triple point and decrease the artifacts caused by the corner as shown in Fig. 5. The Kelvin-Helmholtz instability of the contact discontinuity along the upper wall is clearly visible. These schemes are more robust than the Roe's FDS scheme [8] because no unphysical expansion shock wave on top of the facing step corner occurred in the solutions. It is noted that the scheme can capture the slip line better with a finer grid size.

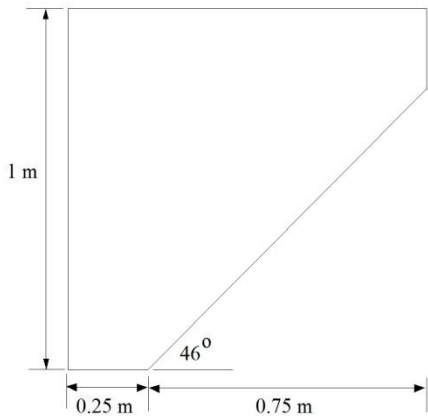


Fig.6. Problem geometry of problem 4.3.

4.3 Mach 2 Shock Reflection over Wedge

The computational domain for a Mach 2 shock reflection over a wedge at 46 degrees [20] is illustrated in Fig. 6. All numerical experiments were performed using a structured triangular mesh with a spacing of 0.0039 for a total of 91,471 cells. Figures 7(a)-(c) show the density contours obtained from the second-order solution accuracy at the four time steps where the shock wave is approximately located at the distance of 0.1 from the right boundary at the time $t = 0.35$.

The solution from the AUSM scheme is improved with good shock and Mach stem resolution until time $t = 0.25$. However, the incident shock is slightly broken-down with spurious and kinked Mach stem due to an inappropriate numerical dissipation added to the vorticity and entropy waves [21] as shown in Fig. 7(c). The slipstream is not shown clearly in these figures. By using the Shadowgraph technique, both the slipstream emanated from the triple point and the spurious and kinked Mach stem are clearly expressed as shown in Fig. 8.

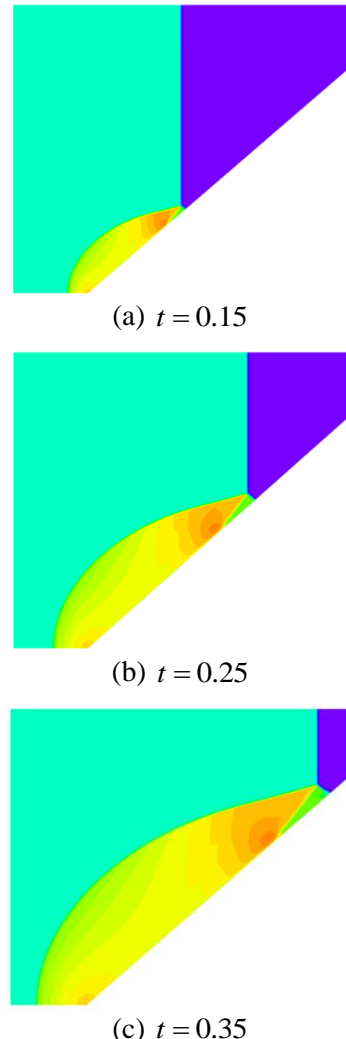


Fig.7. Density contours at four time steps of problem 4.3.

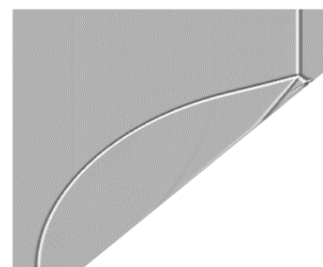


Fig.8. Shadowgraph plot of problem 4.2.

5. Conclusions

In this paper, the AUSM scheme with a reconstruction of the second-order accurate finite volume method on triangular grids in two-dimensional domain was presented. The theoretical formulation of the Euler system of equations, and the discretization of the numerical fluxes were explained in detail. Three high-speed compressible flow examples were used to evaluate the accuracy and the robustness of the scheme. The examination process was found to provide more accurate solutions for two test cases. However, in the last example, the incident shock is slightly broken-down with spurious and kinked Mach stem at time $t=0.35$. In order to improve the solution, the problem is currently investigated to understand the mechanism of these numerical defects.

6. Acknowledgements

The author is pleased to acknowledge the College of Industrial Technology, King Mongkut's University of Technology North Bangkok (KMUTNB), and the National Metal and Materials Technology Center (MTEC) for supporting this research work

7. References

- [1] Zucker, R.D. and Biblarz, O., Fundamentals of Gas Dynamics, 2nd edition, John Wiley & Sons, New Jersey, 2002
- [2] Roe, P.L., Approximate Riemann Solvers, Parameter Vectors, and Difference Schemes, *J. Comput. Phys.*, Vol. 43, pp. 357-372, 1981.
- [3] Perry, K.M. and Imlay, S.T., Blunt-Body Flow Simulations, 24th AIAA/SAE/ASME/ASEE Joint Propulsion Conference, AIAA Paper 88-2904}, 1988.
- [4] Quirk, J.J., A Contribution to the Great Riemann solver Debate, *Int. J. Numer. Meth. Fluids*, Vol. 18, pp. 555-574, 1994.
- [5] Sanders, R. and Morano, E. and Druguet, M. C.}, Multidimensional Dissipation for Upwind Schemes: Stability and Applications to Gas Dynamics, *J. Comput. Phys.*, Vol. 145, pp. 511-537, 1998.
- [6] Pandolfi, M. and D'Ambrosio, D., Numerical Instabilities in Upwind Methods: Analysis and Cures for the "Carbuncle" Phenomenon, *J. Comput. Phys.*, Vol. 166, pp. 271-301, 2001.
- [7] Tang, H., On the Sonic Point Glitch, *J. Comput. Phys.*, Vol. 202, pp. 507-532, 2005.
- [8] Phongthanapanich, S. and Dechaumphai, P., Multidimensional Dissipation Technique for Roe's Flux-Difference Splitting Scheme on Triangular Meshes, *Int. J. Nonlin. Sci. Num.*, Vol. 7, pp. 251-256, 2006.
- [9] Phongthanapanich, S. and Dechaumphai, P., Healing of Shock Instability for Roe's Flux-Difference Splitting Scheme on Triangular Meshes, *Int. J. Numer. Meth. Fluids*, Vol. 59, pp. 559-575, 2009.
- [10] Elling, V., The Carbuncle Phenomenon is Incurable, *Acta Math. Sci.*, Vol. 29B, pp. 1647-1656, 2009.
- [11] Steger, J.L. and Warming, R.F., Flux Vector Splitting of The Inviscid gas Dynamic Equations with Application to Finite Difference Methods, *J. Comput. Phys.*, Vol. 40, pp. 263-293, 1981.
- [12] Van Leer, B., Flux-Vector Splitting for the 1990s, Computational Fluid Dynamics Symposium on Aeropropulsion, AIAA, Cleveland, OH, 1991.
- [13] Liou, M.S. and Steffen, C.J., A New Flux Splitting Scheme, *J. Comput. Phys.*, Vol. 107, pp. 23-39, 1993.
- [14] Frink, N.T., Parikh, P. and Pirzadeh, S., A Fast Upwind Solver for the Euler Equations on Three-Dimensional Unstructured Meshes, AIAA Paper-91-0102, AIAA, 29th Aerospace Sciences

- Meeting and Exhibit, Reno, Nevada, 1991.
- [15] Vekakrishnan V., Convergence to Steady State Solutions of the Euler Equations on Unstructured Grids with Limiters, *J. Comput. Phys.*, Vol. 118, pp. 120-130, 1995.
 - [16] Shu, C.W. and Osher, S., Efficient Implementation of Essentially Non-Oscillatory Shock-Capturing Schemes, *J. Comput. Phys.*, Vol. 77, pp. 439-471, 1988.
 - [17] Linde, T. and Roe, P.L., Robust Euler Codes, 13th Computational Fluid Dynamics Conference, AIAA Paper-97-2098, Snowmass Village, CO, 1997.
 - [18] Woodward, P. and Colella, P., The Numerical Simulation of Two-Dimensional Fluid Flow with Strong Shocks, *J. Comput. Phys.*, Vol. 54, pp. 115-173, 1984.
 - [19] Cockburn, B. and Shu, C.W. The Runge-Kutta Discontinuous Galerkin Method for Conservation Laws V: Multidimensional Systems, *J. Comput. Phys.*, Vol. 141, pp. 199-224, 1998.
 - [20] Takayama, K. and Jiang, Z., Shock Wave Reflection over Wedges: A Benchmark Test for CFD and Experiments, *Shock Waves*; Vol. 7, pp. 191-203, 1997.
 - [21] Phongthanapanich, S. and Dechaumphai, P., Modified H -Correction Entropy Fix for Roe's Flux-Difference Splitting Scheme with Mesh Adaptation, *Trans. Can. Soc. Mech. Eng.*, Vol. 28, pp. 531-549, 2004.